Physics-based forecast modelling of rip-current and shore-break wave hazards

Bruno Castelle[1], Jeoffrey Dehez[2], Jean-Philippe Savy[3], Sylvain Liquet[4], and David Carayon[2]

[1]Univ. Bordeaux, CNRS, Bordeaux INP, EPOC, UMR 5805, F-33600 Pessac, France
[2]INRAE Nouvelle Aquitaine, Cestas-Gazinet, France
[3]SMGBL, Messanges, France
[4]Météo-France, Toulouse, France

Correspondence: Bruno Castelle (bruno.castelle@u-bordeaux.fr)

Abstract. Sandy beaches are highly attractive but also potentially dangerous environments for those entering the water as they can expose to physical hazards in the surf zone. The most severe and widespread natural hazards on beaches are rip currents and shore-break waves, which form under different wave, tide and morphological conditions. This paper introduces two new, simple, physics-based rip-current and shore-break wave hazard forecast models. These models, which depend on a limited

5 number of free parameters, allow to compute the time evolution of the rip current flow speed V and shore-break wave energy E_{sb}. These models are applied to a high-energy meso- macro-tidal beach, La Lette Blanche, in southwest France where intense rip currents and shore-break wave hazards co-exist. Hourly lifeguard-perceived hazards collected during the patrolling hours (from 11AM to 7PM) from July 1 to August, 2022 are used to calibrate the two models. This data is also used to transform V and E_{sb} into 5-level scale from 0 (no hazard) to 4 (hazard maximized). The model accurately predicts rip-current and shore-

10 break wave hazard levels, including their modulation by tide elevation and incident wave conditions, opening new perspectives to forecast multiple surf-zone hazards on sandy beaches. The approach presented here only requires a limited number of basic beach morphology metrics, and allows the prediction of surf-zone hazards on beaches where wave forecast is available.

1 Introduction

Predicting natural hazards, such as e.g. flash floods, wildfires, and hurricanes, and disseminating warnings based on those

15 predictions is crucial to protect property and natural resources, but also to protect people from injury and death (National Research Council, 1991; Merz et al., 2020; Bates et al., 2021). Over the last decades, prediction capabilities of atmospheric and hydrologic hazards, often referred to as weather-related natural hazards, have been greatly increased (e.g. Brunner et al., 2021). While a lot of scientific effort and media coverage involve e.g. hurricanes (Gall et al., 2013), coastal flooding (Stockdon et al., 2023) or flash floods (Corral et al., 2019), in comparison less attention has been paid to the surf-zone hazards beachgoers

20 expose themselves to. However, in the USA, rip currents on surf beaches were the third-leading cause of weather-related deaths from 2012 to 2021 according to the National Weather Service (US Department of Commerce), not far behind heat waves and flooding. Contrary to most of these other weather-related natural hazards (e.g. Zscheischler et al., 2020), surf-zone hazards are not necessarily related to extreme events as fatal drowning and severe injuries at the beach predominantly occur during fair

weather conditions, i.e. typically during warm, sunny and light-wind days (Dwight et al., 2007; Ibarra, 2011; Coombes et al.,
25   2009; de Korte et al., 2021; Castelle et al., 2024). Therefore, improving our predicting capacity of surf-zone hazards on beaches is critical to reduce the burden of fatal drownings (Dusek and Seim, 2013) as well as that of other types of injuries.

Sandy beaches offer abundant recreational opportunities, tourism potential, and valuable ecosystem services (Ghermandi and Nunes, 2013; Hall and Page, 2014; Bujosa et al., 2015; West, 2019), including activities such as bathing and wading (Britton et al., 2018; Wood et al., 2022; Dehez and Lyser, 2024). However, beachgoers may face physical hazards within the

30   surf zone. Among the most significant and widespread natural hazards leading to surf-zone injuries (SZI), including drowning incidents, are rip currents (MacMahan et al., 2006; Dalrymple et al., 2011; Castelle et al., 2016; Houser et al., 2020) and shore-break waves (Chang et al., 2006). Rip currents are narrow, seaward-flowing currents that originate in the surf zone, often near the waterline, extending through the breakers and sometimes beyond. These currents are a primary cause of unintentional drownings on many surf beaches worldwide (e.g. Brighton et al., 2013; Arozarena et al., 2015; Barlas and Beji, 2016; Li, 2016;

35   Castelle et al., 2018; Brewster et al., 2019), as they can carry bathers offshore into deeper water, leading to drowning through exhaustion or panic (Brander and Short, 2001; Drozdzewski et al., 2012). Rip currents are driven by depth-induced breaking wave energy dissipation, although their formation mechanisms can vary (Castelle et al., 2016). The most common rip type flows through channels carved into nearshore sandbars (e.g. Houser et al., 2013) on intermediate beaches (Wright and Short, 1984). These channel rips are caused by alongshore variations in breaking wave energy dissipation due to alongshore-variable sandbar

40   depths (Bowen, 1969; Haller et al., 2002; Bruneau et al., 2011). Rip current activity typically increases with shore-normal wave incidence, higher wave height, longer wave period (e.g. Austin et al., 2010; Drønen et al., 2002; Bruneau et al., 2011; Winter et al., 2014; MacMahan et al., 2006), and lower tide level (Aagaard et al., 1997; MacMahan et al., 2005; Brander and Short, 2001; Houser et al., 2013; Castelle et al., 2020). Shore-break waves, in contrast, are plunging or dumping waves that break close to the shore on steep beach faces, causing a wide range of injuries, including severe spinal injuries (Chang et al., 2006;

45   Robbles, 2006; Puleo et al., 2016; Castelle et al., 2018; Griepp et al., 2022). Most injuries associated with shore-break waves result from wave-induced impacts, followed by shallow water diving incidents, the latter often involving surfers (Thom et al., 2022). Unlike rip currents, research on shore-break waves is limited, mostly due to the challenges of quantifying their energy and impact forces on the human body. Castelle et al. (2024) observed that lifeguards in southwest France perceive shore-break wave hazards to be greater during long-period, near shore-normal waves and higher tides. Furthermore, prior studies indicate

50   that the occurrence of spinal injuries from shore-break waves increases with long-period waves, and higher water level as waves typically break on the steepest sections of the beach (Castelle et al., 2019).

Despite our increased understanding in rip current dynamics, a limited number of rip current hazard forecast systems have been developed over the last decade. The approaches include for instance process-based modelling (Austin et al., 2013, which requires detailed information of the beach morphology); statistical modelling of the likelihood of hazardous rip current using

55   either lifeguard estimation of rip flow speed (Dusek and Seim, 2012, 2013) or measured rip-flow speed (Moulton et al., 2017a); physics-based parametrisation of channel rip flow speed (Casper et al., 2024); hazard levels based on empirical thresholds in tide elevation, wave height and period (Scott et al., 2022). While some of these models skilfully predict rip current hazard levels, they have been validated on a limited number of beaches. Additional rip flow speed and/or lifeguard-perceived and/or

topo-bathymetric datasets therefore need to be collected. In addition, these surf-zone hazard models only consider rip currents, while on some beaches the most threatening hazard is shore-break waves (e.g. Puleo et al., 2016). This calls for more generic surf-zone hazard models to be applied to a wide range of sandy beaches.

In this contribution, we present two simple physics-based rip-current and shore-break wave hazard forecast models which are validated at a high-energy sandy beach in southwest France, where strong rip currents and hazardous shore-break waves co-exist (Castelle et al., 2024) and are largely the most important cause of SZIs (Castelle et al., 2018). In Section 2 the field site and the 2-month dataset of environmental conditions and lifeguard-perceived hazard data used for model calibration are presented. Section 3 explains the development of the rip-current and shore-break wave hazard models. Results are given in Section 4, which are further discussed in Section 5. We show that the two models skilfully predict the lifeguard-perceived rip-current and shore-break wave hazards, including their complex modulation by tidal elevation, incident wave energy and neap-spring tide cycles. These simple physics-based models providing quantitative estimate of rip-flow speed and shore-break wave energy, and associated 5-level scale hazard rating, only require a limited number of time-invariant free parameters. These parameters can be either given thanks to some basic knowledge of the beach morphology, or through calibration using e.g. lifeguard-perceived hazard data. The proposed framework offers new opportunities for forecasting rip-current and shore-break wave hazards at surf beaches with available wave predictions.

2 Field site and data

2.1 La Lette Blanche Beach

La Lette Blanche beach (Figure 1b) is representative of the majority of open coast beaches in southwest France. Its typical beach state is intermediate and double-barred, with crescentic patterns on the inner intertidal bar and a transverse bar and rip morphology on the outer subtidal bar. The spacing between inner-bar rip channels is on average approximately 400 m. This beach is situated in a meso-macrotidal environment, with an average tidal range of 2.6 m and a maximum of 4.4 m. It is exposed to high-energy ocean waves generated in the North Atlantic, with a summer-mean (July-August) significant wave height H_s of about 1.1 m and a peak wave period T_p of 9 s. Like other open beaches in the region, rip current are ubiquitous (Figure 1c), with strong channel rips flowing through the inner-bar rip channels (Bruneau et al., 2009). Rip current activity peaks around mean low tide level under energetic, shore-normal wave conditions (e.g. Bruneau et al., 2011), which coincide with a higher occurrence of drowning incidents and rescues in southwest France (Castelle et al., 2019; de Korte et al., 2021; Castelle et al., 2024). Additionally, a significant number of mild to severe injuries in the surf zone are caused by shore-break waves (Figure 1c, Castelle et al., 2018). Research has shown that these injuries are more frequent during higher water levels and large tidal ranges when waves break over the steepest sections of the beach profile (Castelle et al., 2019, 2024).

La Lette Blanche beach is monitored by lifeguards during the summer months (July and August) between 11 AM and 7 PM. During these hours, a supervised bathing zone, typically less than 100 m wide, is established between two red and yellow flags (Figure 1b). This zone is strategically located away from potential rip currents. Due to the large tidal range, which causes rapid changes in the location, intensity, and nature of surf zone hazards, lifeguards may relocate the supervised bathing zone

multiple times throughout the day. To communicate surf zone hazards, lifeguards use a color-coded flag system that reflects their assessment of conditions, including rip currents and shore-break waves: (1) a green flag indicates supervised bathing with no significant physical hazard; (2) a yellow-orange flag signifies dangerous but supervised bathing; and (3) a red flag means

95   bathing is prohibited.

Figure 1. (a) Location map of La Lette Blanche beach, southwest France and (b) view from the lifeguard station on the top of the dune on July 14, 2022, 12PM (Ph. B. Castelle). Photographs in southwest France of the two major surf-zone hazards with (c) rip currents (Ph. Observatoire de la Côte de Nouvelle-Aquitaine) and (d) shore-break waves (Ph. SMGBL).

2.2 Summer 2022 field experiment

During the boreal summer of 2022, from July 1 to August 31, a beach safety field experiment was carried out at La Lette Blanche beach. This study generated a unique multidisciplinary database encompassing various aspects such as beachgoer surveys, surf-zone drifter measurements, topographic surveys, lifeguard assessments of surf-zone hazards and beach crowds, as well as monitoring of environmental conditions. For further details on these datasets, please refer to Dehez et al. (2024) and Castelle et al. (2024).

In the present contribution, we use only lifeguard-perceived surf-zone hazards and wave and tide conditions. Given that the aim of the present contribution is to eventually operate surf-zone hazard forecast, in contrast with Castelle et al. (2024) we used numerical wave hindcast instead of in situ offshore wave measurements. The numerical wave hindcast consisted in an analysis of the high-resolution wave forecast model WaveWatch 3, developed by NOAA (Tolman et al., 2002), forced by winds from the ARPEGE model of Météo-France, over the Atlantic domain. WaveWatch 3 uses an unstructured grid (Roland and Ardhuin, 2014), allowing the French coasts to be described with a resolution of approximately 200 m. Different coastal processes are represented in this model, as unified parameterization of wave breaking from offshore to coast, wave reflection at the coast, refraction due to currents and bathymetry, and bottom friction in front of La Lette Blanche beach. Modelled wave conditions were extracted in approximately 10-m depth. The data was further compared with the wave measurements at the directional wave buoy located approximately 80 km further north in 50-m depth, which in previous work was assumed representative of the wave conditions given the overall open and straight nature of the coast. Results show a root-mean-square error (RMSE), coefficient of determination (r^2) and bias of 0.17 m, 0.91 and -0.03 m. These metrics provide confidence into both model skill and the relevance of the wave buoy measurements used in previous work. In addition, tide conditions at the beach were estimated using the TPXO9 (version 5) $1/30°$-resolution atlas (Egbert and Erofeeva, 2002) at the grid point the closest to La Lette Blanche beach. Figure 2a-d displays the wave and tide conditions during the 2022 experiment, showing significant wave height H_{s0} (peak wave period T_p) ranging from 0.30 m to 2.19 m (3.85 s to 19.38 s) with a mean of 0.96 m (9.21 s). Waves were predominantly from the west-northwest, with the average angle of wave incidence with respect to shore-normal of $23.39°$. Nearly 2.5 neap-spring tide cycles were covered (Figure 2d), with the daily tide range (TR) ranging 1.39–4.06 m with a mean of 2.73 m.

During each patrolled day of the summer 2022 beach safety experiment, the chief lifeguard (or the co-chief on the chief lifeguard's days off, two days a week) provided hourly estimates of rip current hazard (HR_l) and shore-break wave hazard (HS_l). These hazards were rated on a 5-level scale ranging from 0 (no hazard) to 4 (maximum hazard). Lifeguards were instructed to assess the environmental hazard level rather than the risk, meaning the focus was on the inherent hazard conditions rather than the likelihood of water users exposing themselves to rip currents or shore-break waves. Figure 2e,f illustrates the time series of daily-mean lifeguard-estimated rip current hazard ($\overline{RH_l}$) and shore-break wave hazard ($\overline{SH_l}$). The data indicate that the daily average rip current hazard generally increases with larger, longer-period, and near shore-normal waves. In contrast, the shore-break wave hazard is heightened under conditions of long-period, near shore-normal waves and large tidal ranges (Castelle et al., 2024).
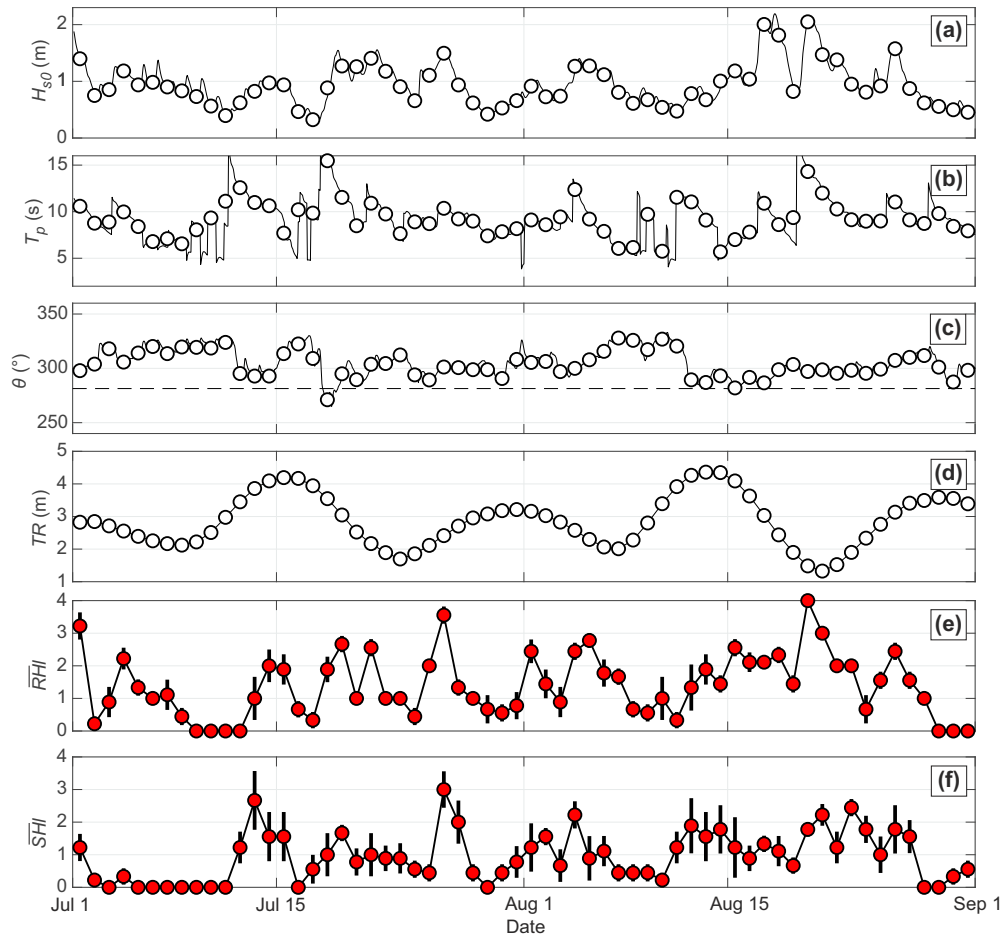
Figure 2. Time series of environmental conditions in nearly 10-m depth offshore of the study site and lifeguard-estimated surf-zone hazards during patrolling hours (11AM-7PM): (a) significant wave height H_{s0} in 10-m depth; (b) peak wave period T_p; (c) angle of wave incidence θ; (d) tide range TR; daily-mean (e) lifeguard-perceived rip-current hazard $\overline{RHl}$ and (f) lifeguard-perceived shore-break-wave hazard $\overline{SHl}$. In all panels the circles indicate the daily mean, and in (e,f) the vertical lines indicate the daily standard deviation.

3 Physic-based hazard models

3.1 Rip current

Rip current hazard can be estimated through the rip flow speed. Here we consider an idealised rip-channelled beach on which breaking waves drive a rip current through the deeper channel (Figure 3). Channel rips are essentially driven by the alongshore variation in breaking-wave-energy dissipation due to the alongshore variability in depth of the sandbar. This can be simplified into the alongshore pressure gradients in the surf zone dS/dx, with x the longshore coordinate and S the wave set-up i.e. the increase in mean water level driven by wave breaking. These alongshore pressure gradients drive feeder currents converging at

the channels and turning offshore as rip currents (Haller et al., 2002). There is a wealth of empirical formulas derived from field and laboratory measurements to estimate wave set-up (Gomes da Silva et al., 2020). A popular, simple, formula gives the wave set-up S at the shoreline as a function of offshore significant wave height H_s only (Guza and Thornton, 1981; Raubenheimer

140 et al., 2001; Atkinson et al., 2017):

$$S \approx 0.16 H_s \tag{1}$$

The rip-current flow is therefore controlled by the alongshore pressure gradient between the wave set-up immediately on-shore of the bar/rip system in the alignment of the bar S_b and of the channel S_c (Figure 3c). By assuming Equation (1), but looking immediately onshore of the bar/rip system instead of the waterline where the entire incident wave energy has been

145 dissipated, we can assume $S_b = 0.16 \Delta H_{sb}$ and $S_c = 0.16 \Delta H_{sc}$, where ΔH_{sb} and ΔH_{sc} are the decrease in wave height due to depth-induced breaking across the bar and the channel, respectively (Figure 3b). The significant wave height H_{s0} in 10-m depth was transformed into significant wave height at breaking H_s using the direct formula of Larson et al. (2010). Critical to both ΔH_{sb} and ΔH_{sc} is the the depth-induced breaking wave height decay law. Here we consider simple first-pass estimation of the significant wave height decay for irregular waves (Figure 3d), for $h > 0$ and $H_s > \gamma h$ (broken waves):

$$150 \quad \Delta H_s = (H_s - \gamma h)^2 / H_s^2 \tag{2}$$

where h is the water depth of the bar or channel, and γ is the breaker index.

By neglecting the bottom friction and assuming steady flow, the depth- and time-averaged alongshore momentum balance can be written as:

$$\frac{\partial}{\partial x}(U^2 h) + \frac{\partial}{\partial y}(UVh) = -gh\frac{\partial S}{\partial x} \tag{3}$$

155 where g is the gravitational acceleration. The right-hand (left-hand) side of equation (3) can be approximated as $2V^2/w$ $(-gh(S_c - S_b)/w)$, where V is the rip-flow velocity, leading to:

$$V \approx \sqrt{\frac{g(S_b - S_c)}{2}} \tag{4}$$

where $S_b = 0.16 \Delta H_{sb}$ and $S_c = 0.16 \Delta H_{sc}$ the wave set-up onshore of the bar and of the channel, respectively.

This simple rip-flow model proceeds as follow : at each time step, rip flow speed $V(t)$ is computed as a function of $S_b(t)$

160 and $S_c(t)$, based on the significant wave height at breaking $H_s(t)$ and the local water depth across the bar (channel) $h_b(t) = z_{bar} + \eta(t)$ ($h_c(t) = z_{bar} + d + \eta(t)$), with $\eta(t)$ the tide elevation, z_{bar} the elevation of the sandbar and d the channel depth (Figure 3b). The rip flow model V includes only three time-invariant free parameters that need to be calibrated and/or inferred from field data : the breaker index γ, the sandbar elevation z_{bar} and the channel depth d.
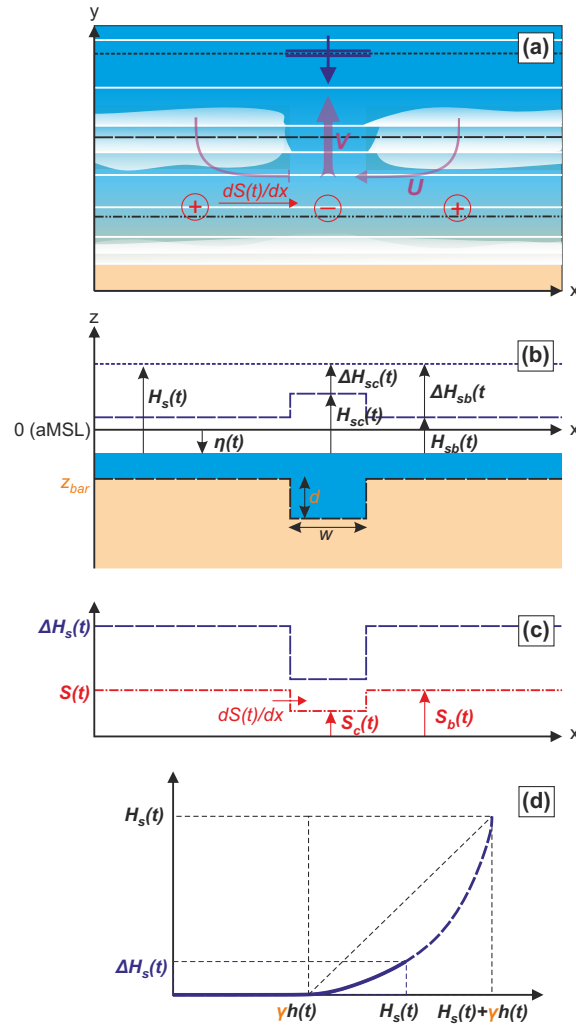
Figure 3. Schematics of the physics-based rip-current flow model: (a) top-view schematics of a rip-channelled beach with a rip current flowing through the deeper channel driven by the depth-induced wave breaking alongshore pressure gradients dS/dx; (b) alongshore section with significant wave height at breaking H_s, across the bar H_{sb} and across the channel H_{sc}, and their corresponding decrease with respect to breaking ΔH_{sb} and ΔH_{sc}; (c) corresponding alongshore-variable wave set-up S across the bar S_b and across the channel S_c, and resulting alongshore pressure gradient $dS/dx \approx (S_b - S_c)/w$; (d) idealised significant wave height decay model ΔH, for a given H_s, water depth h with γ the breaker parameter. In all panels, the time-invariant free model parameters are indicated in orange.

3.2 Shore-break

165   We used a similar, simple, physics-based approach to estimate shore-break wave hazard. Contrary to rip flow speed there is no theoretical framework to estimate a measure of the shore-break wave energy. The presence of shore-break waves can be estimated through the dimensionless Irribarren parameter Ir which is a proxy for break type (Battjes, 1974):

$$Ir = \tan\beta / \sqrt{H_{ssb}/L_0} \tag{5}$$

where $L_0 = gT_p/2\pi$ is the deep water wavelength, $\tan\beta$ is the local beach slope and H_{ssb} is the significant wave height
170 upon shore breaking. While breaking goes from spilling to collapsing through plunging as Ir increases, it does not provide
information of the power of the breaking waves. Therefore, we introduce a shore-break wave energy parameter $E_{ssb} = IrH_{sb}^2$,
which therefore reads :

$$E_{sb} = H_{ssb}^{3/2} T_p g^{1/2} \tan\beta \tag{6}$$

In order to compute E_{sb}, a beach profile and a wave height model is required. Here we consider an idealised Dean profile
175 given by $z = 5 + ax^b$, which together with the tide elevation is used to compute the beach slope $\tan\beta(\eta)$ (Figure 4a). Critical
to E_{sb} is the shore-break wave height H_{ssb}. Similar to all intermediate beaches, the beaches in southwest France are barred,
with depth-induced breaking wave energy dissipation across the offshore sandbar limiting the breaking wave height at the
shore, especially for lower tides. The sandbar was mimicked by assuming a terrace with a given elevation Z_l (Figure 4a)
where waves may dissipate before reaching the shore. Therefore, consistent with the rip current model, the wave height decay
180 $\Delta H_s = H_s - H_{ssb}$ was determined through a simple wave height decay law (Figure 4b).

This simple shore-break wave energy model proceeds as follow : at each time step, the beach slope $\tan\beta(\eta(t))$ and the
shore-break wave height H_{ssb}(t) are computed. If $\eta(t) < Z_l$ during the lower tides, the sandbar is emerged and all the wave
energy is dissipated offshore, meaning $H_{ssb}(t) = 0$. At the other end of the spectra, if $H_s(t) > \gamma_s(\eta(t) - Z_l)$ with γ_s the
breaker parameter of the shore-break model, there is no wave breaking offshore and $H_{ssb}(t) = H_s(t)$. In between, offshore
185 wave breaking occurs resulting in a decreased shore-break significant wave height by ΔH_s (Figure 4b) resulting in:

$$H_{ssb}(t) = H_s(t) - \frac{[H_s(t) - \gamma_s(\eta - Z_l)]^2}{H_s(t)} \tag{7}$$

The shore-break wave energy model includes four time-invariant free model parameters : a and b describing the beach profile
shape, as well as γ_s the breaker parameter and Z_l the terrace elevation.
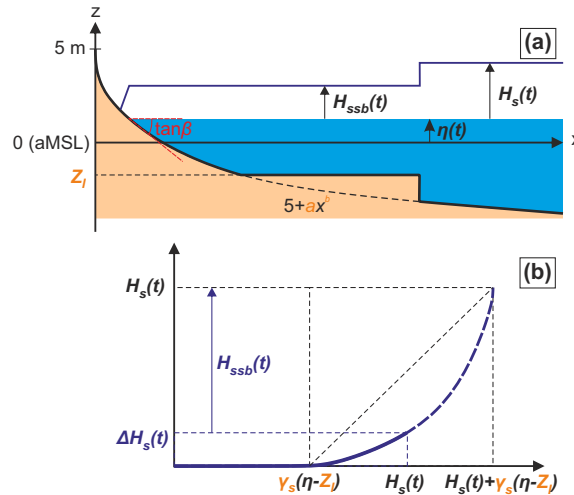
Figure 4. Schematics of the physics-based shore-break wave energy model: (a) Idealised beach profile based on a Dean profile $z = 5 + ax^b$ and a superimposed bar with $z >= Z_l$, resulting in the shore-break significant wave height H_{ssb} that depends on (b) the offshore significant wave height H_s and depth-induced breaking significant wave height decay ΔH_s. In all panels, the time-invariant free model parameters are indicated in orange.

3.3 Model calibration and transformation into a 5-level scale hazard

190 A two-step approach was used, both steps using the lifeguard-perceived surf-zone hazard data RHl (rip current) and HSl (shore-break wave): (1) calibration of the free parameters of V and E_{sb} and (2) a quantile-quantile approach to transform V and E_{sb} into a 5-level scale hazard. First, a large set of simulations were run for a wide range of free parameters. The optimal parameters were found by maximizing the coefficient of determination r^2 between V (E_{sb}) and RHl (SHl) during patrolling hours from 11AM to 7PM during the entire summer of 2022. Second, the values of V and E_{sb} concurrent to lifeguard

195 observations were sorted and thresholds were computed in order to obtain the same number of modelled hazard levels (Table 1). Based on these ranges of V and E_{sb}, the complete time series of V and E_{sb} were transformed into modelled rip-current (RHm) and shore-break wave (SHm) hazard on the same 5-level scale as for lifeguard observations. The accuracy of these predictors was further addressed through confusion matrices. In addition, the modelled daily-mean rip-flow speed V (shore-break wave energy E_{sb}) and the modelled daily-mean rip-current hazard $\overline{RHm}$ (shore-break wave hazard $\overline{SHm}$) were also

200 compared with daily-mean lifeguard-perceived rip current hazard $\overline{HRl}$ (shore-break wave hazard $\overline{HRl}$) in order to address the ability of the two models to predict high-hazard days.

Table 1. Number of hourly lifeguard-perceived hazard observation n (rip current : RHl, shore-break wave : SHl) discriminated by level (from 0 to 4) over a total of 558 hourly observations, together with the corresponding range of V and E_{sb}.

Hazard level	$n(RHl)$	V range (m/s)	$n(SHl)$	E_{sb} range (m^2)
0	146	$V < 0.15$	282	$E_{sb} < 0.49$
1	167	$0.15 \leqslant V < 0.46$	105	$0.49 \leqslant E_{sb} < 0.77$
2	144	$0.46 \leqslant V < 0.69$	102	$0.77 \leqslant E_{sb} < 1.34$
3	83	$0.69 \leqslant V < 0.95$	56	$1.34 \leqslant E_{sb} < 2.10$
4	18	$V \geqslant 0.95$	13	$E_{sb} \geqslant 2.10$

4 Results

4.1 Rip current hazard modelling

The best pearson correlation ($r = 0.77$) between the modelled rip-flow speed V and the hourly lifeguard-perceived rip-current
205 hazard RHl was obtained for $\gamma = 0.23$, $z_{bar} = -3$ m and $d = 6.5$ m. Figure 5a shows the corresponding V against RHl. It shows that RHl increases with increasing V and that for all hazard levels the values are nearly normally distributed, except for $RHm = 0$, which is clearly biased towards $V = 0$. The corresponding confusion matrix (Figure 5b) indicates that over the 558 hourly lifeguard-perceived hazard observations, 308 are correctly classified by the model. In line with the quantile approach used, the confusion matrix is symmetric, with a resulting accuracy of 0.55. However, by merging $RHm = 0, 1$ into low-hazard
210 and $RHm = 2, 3, 4$ into moderate- to high-hazard hours (Figure 5c), the accuracy increases to 0.83, with a F-Score of 0.81, meaning that the model accurately predicts moderate to high rip-current hazard hours.

Natural Hazards
and Earth System
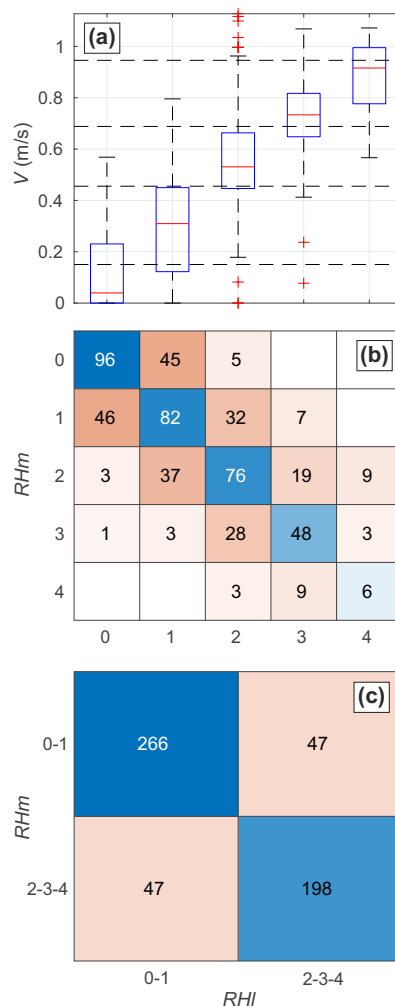
Figure 5. (a) Box plot of the modelled hourly rip-flow speed V versus hourly lifeguard-perceived rip-current hazard RHl on a 5-level scale. The central horizontal red marks indicate the median, the bottom and top edges of the box indicate the 25th and 75th percentiles, respectively, the whisker length indicates 1.5 times the interquantile range, and the crosses are the outliers. The horizontal dashed lines represent the limits between each hazard-perceived scale using a quantile-quantile approach. Corresponding confusion matrix of (b) hourly modelled (SHm) and lifeguard-perceived (RHl) rip-current hazard on the 5-level scale and (c) further discriminating low (RH=0,1) and moderate to high (RH=2,3,4) rip-current hazard hours.

Figure 6 shows the time series of wave and tide conditions as well as of the modelled rip-flow speed V, hourly modelled rip-current hazard level RHm and hourly lifeguard-perceived rip-current hazard level RHl. Results show that V is strongly modulated by tidal elevation η, with increased rip-current hazard for lower tidal elevations. On longer timescales, modelled rip current hazard is also modulated by the incident wave energy, with modelled hazard increasing with increasing wave height and wave period. Figure 6d,f,h further zooms onto a moderate-energy, average tide range, 5-day window showing that the tidal

modulation of the lifeguard-perceived rip-current hazard is very well captured by the model (Figure 6h). During a five-day period comprising the onset of a high-energy wave event with H_s exceeding 2 m, the model also well captures the rip-current hazard which is maximised throughout August 20 (Figure 6e,g,h), which was also the only day of the summer of 2022 when the red flag was hoisted at La Lette Blanche beach, with lifeguard-perceived rip-current hazard maximized throughout the day.
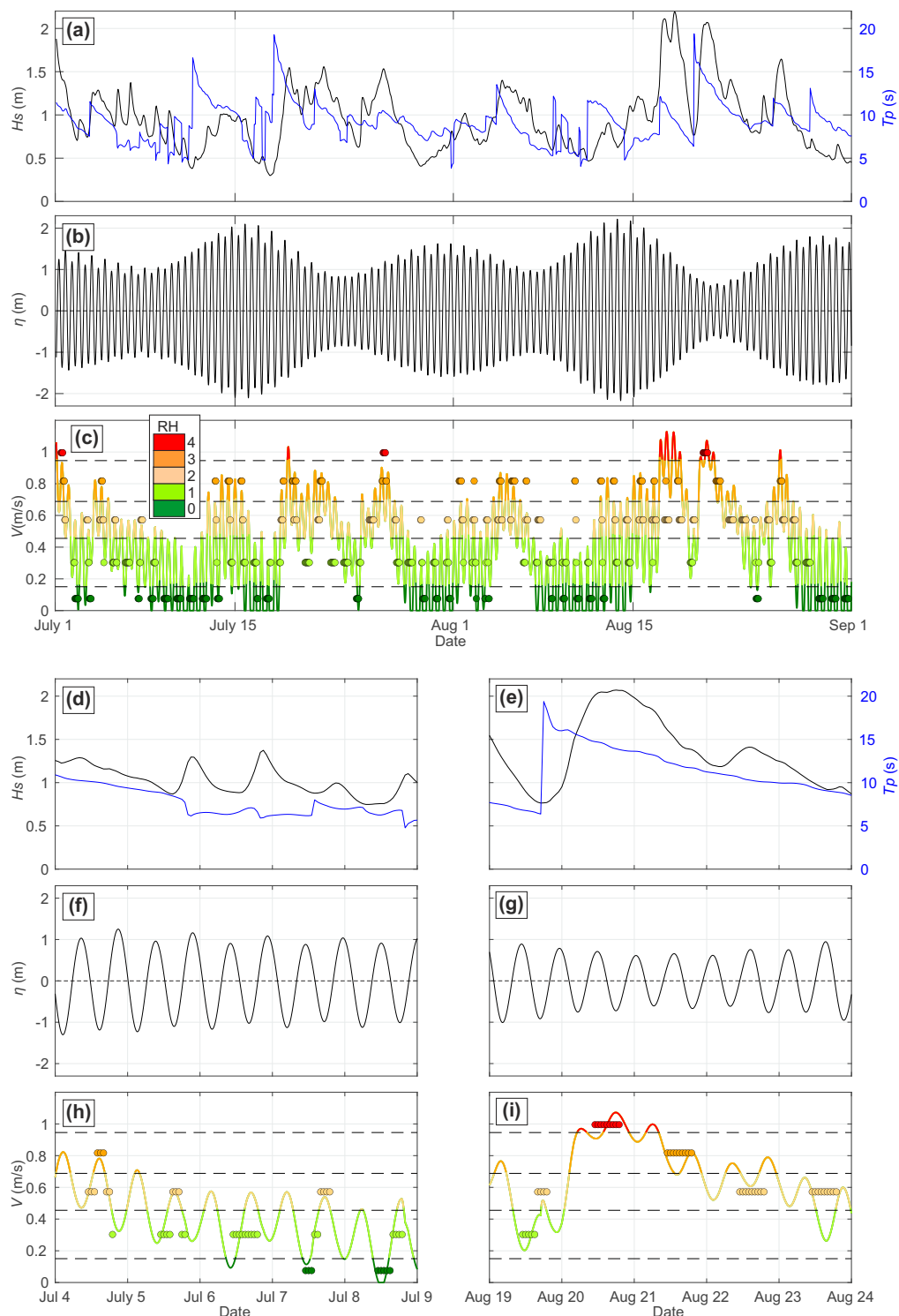
Figure 6. Time series of (a) significant wave height in 10-m pdeth H_{s0} and peak wave period T_p; (b) astronomical tide level η; (c) modelled rip-current flow speed V and its corresponding hazard level RHm (coloured line) and lifeguard-perceived rip-current hazard RHl (coloured circles), which are further zoomed onto a 5-day period of (d,f,h) moderate-energy waves and average tide range and (e,g,i) high-energy waves and neap tides.

Figure 7 also shows that the model accurately predicts daily mean rip-current hazards. The pearson correlation between the daily-mean modelled RHm and lifeguard-perceived RHl hazards reaches $r = 0.82$. The model well captures most of the high-hazard days, although some are overestimated (e.g. August 17) or underestimated (July 28). The model also tends to slightly overestimate the daily-mean hazard during days when lifeguards perceived no rip-current hazard throughout the patrolling hours.
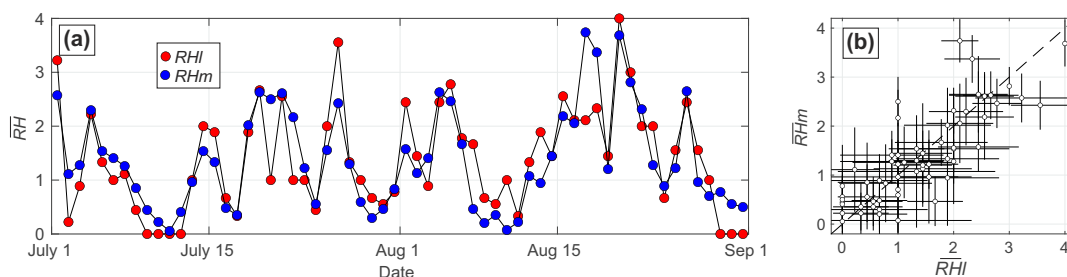
Figure 7. (a) Time series of daily-mean modelled (blue, $\overline{RH}m$) and lifeguard-perceived (red, $\overline{RH}l$) rip-current hazard on the 5-level scale. (b) Corresponding plot of $\overline{RH}m$ versus $\overline{RH}l$ with the horizontal and vertical lines indicating their daily standard deviation.

4.2 Shore-break wave hazard modelling

The best pearson correlation ($r = 0.71$) between the modelled shore-break wave energy E_{sb} and the hourly lifeguard-perceived shore-break wave hazard RHl was obtained for $a = -2.75$, $b = 0.3$, $\gamma_s = 0.4$ and $Z_l = -2$ m. Figure 8a shows that SHl increases with increasing E_{sb} with, for all hazard levels, values nearly normally distributed. In contrast with rip-current hazard results, which showed a limited number of outliers (Figure 5a), outliers are found for all lifeguard-perceived shore-break wave hazard levels SHl, except for $SHl = 1$. The corresponding confusion matrix (Figure 5b) shows that over the 558 hourly lifeguard-perceived hazard observations, 299 are correctly classified by the model, resulting in an accuracy of 0.54. However, and in line with what was found for rip-current hazard, by merging $SHm = 0, 1$ into low-hazard and $SHm = 2, 3, 4$ into moderate- to high-hazard hours (Figure 5c), the accuracy increases to 0.83 with a F-Score of 0.72, meaning that the model skilfully predicts the hours with moderate to high shore-wave break hazard.
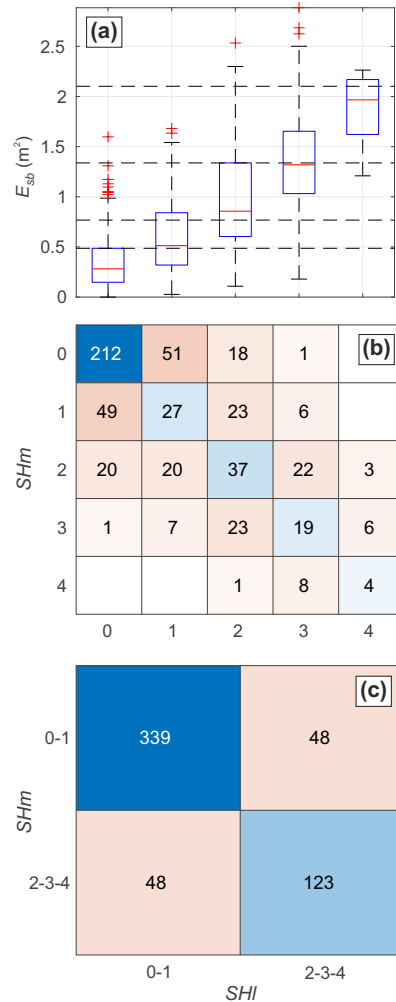
Figure 8. (a) Box plot of the hourly modelled shore-break wave energy E_{sb} versus hourly lifeguard-perceived shore-break wave hazard SHl on a 5-level scale. The central horizontal red marks indicate the median, the bottom and top edges of the box indicate the 25th and 75th percentiles, respectively, the whisker length indicates 1.5 times the interquantile range and the crosses are the outliers. The horizontal dashed lines represent the limits between each hazard-perceived scale using a quantile-quantile approach. Corresponding confusion matrix of (b) hourly modelled (SHm) and lifeguard-perceived (SHl) shore-break wave hazard on the 5-level scale and (c) further discriminating low (SH=0,1) and moderate to high (SH=2,3,4) shore-break wave hazard hours.

Figure 9 shows the time series of wave and tide conditions, as well as of the modelled shore-break wave energy E_{sb} and hazard level SHm, and hourly lifeguard-perceived shore-break wave hazard SHl. Results show that E_{sb} is strongly modulated by the tidal elevation η with, in contrast with rip-current hazard, shore-break wave hazard maximized during the higher stage of the tide. In line with rip-current hazard, on longer timescales shore-break wave hazard increases with increased incident wave energy. Figure 9d,f,h further zooms onto a moderate-energy 5-day period moving from moderate to spring tides, showing

that the tidal modulation of the lifeguard-perceived shore-break wave hazard SHl and the increased hazard with increased tide range are well captured by the model (Figure 9h). During a five-day period comprising the progressive decay in incident wave energy during nearly steady neap-moderate tides, the model also well captures the progressive decrease of shore-break wave hazard at high tides.
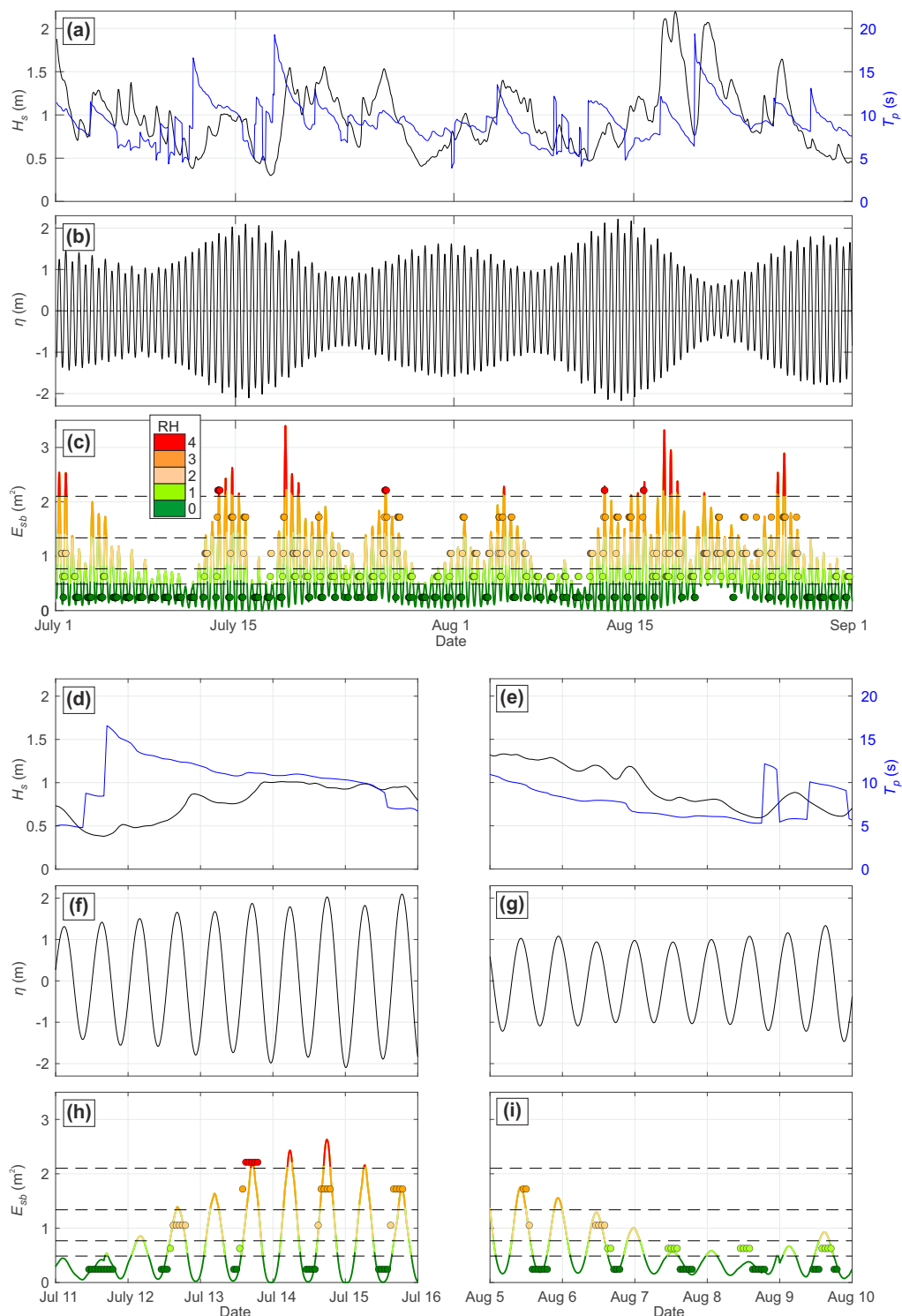
Figure 9. Time series of (a) significant wave height in 10-m depth H_{s0} and peak wave period T_p; (b) astronomical tide level η; (c) modelled shore-break wave energy E_{sb} and its corresponding hazard level (coloured and circles), which are further zoomed onto a 5-day period of (d,f,h) moderate-energy waves and spring tides and (e,g,i) decreasing energy waves and neap tides.

245   Figure 10 also shows that the model accurately predicts daily-mean shore-break wave hazards. The pearson correlation r between daily-mean modelled shore-break wave hazard SHm and daily-mean lifeguard-perceived shore-break wave hazard SHl is 0.74. The model well captures most of the high-hazard days, although the two days with the highest lifeguard-perceived shore-break wave hazard (July 13 and July 26) are slightly underestimated by the model.
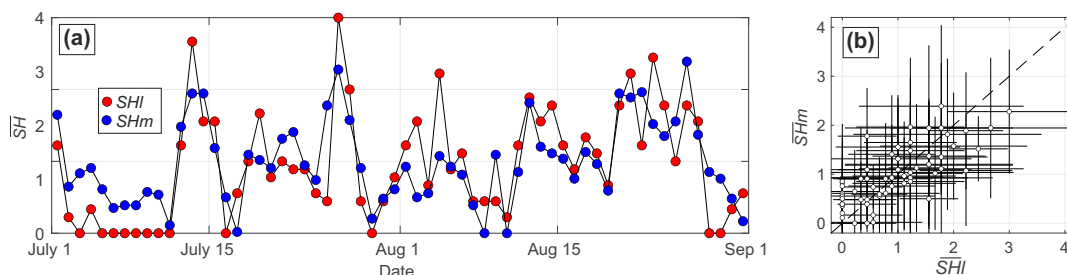
Figure 10. (a) Time series of daily-mean modelled (blue, $\overline{SHm}$) and lifeguard-perceived (red, $\overline{SHl}$) shore-break wave hazard on the 5-level scale. (b) Corresponding plot of $\overline{SHm}$ versus $\overline{SHl}$ with the horizontal and vertical lines indicating their daily standard deviation.

5   Discussion

250 Two simple physics-based rip current and shore-break wave hazard models were developed and further calibrated and tested on a high-energy meso- macro-tidal beach where the two surf-zone hazards co-exist. Previous beach hazard predictors essentially focused on rip currents with, to the best of our knowledge, only Casper et al. (2024) proposing a physics-based formulation. Their approach, based on the pioneering work of Moulton et al. (2017b), is consistent with the rip-flow model proposed here as it considers an idealised bar-rip morphology and the alongshore gradient in breaking-wave-driven-setup as the driving

255 mechanism for rip current flow. In contrast with Moulton et al. (2017b) and Casper et al. (2024) our rip-flow model (1) is more simple as it does not discriminate between different surf zone conditions (shore-break, bar-break or saturated in Moulton et al., 2017b) and (2) has a smaller number of free parameters. A detailed comparison between the two models should be performed on different beaches to address for which type of morphological, tide and wave conditions a model performs better or worse. In addition, here based on lifeguard-perceived hazard on a 5-level scale, modelled rip flow speed V was transformed into a similar

260 hazard scale, showing very good skill (accuracy and F-Score exceeding 0.8) to predict moderate to high hazard hours ($RHl = 2, 3, 4$). The computed accuracy and F-Score are very good, and trying to further improve these metrics by complexifying the model may not be relevant. Indeed, as beach safety professionals, lifeguards are supposed to develop a more robust hazard perception than laypersons (Sandman et al., 1987; Slovic, 1999). However, according to Rowe and Wright (2001), it can also be argued that lifeguards remain human beings whose hazard perception can influenced by personal factors (experience, gender,

265 etc.). Using average lifeguard-perceived hazard data from all the lifeguards on duty, instead of the chief lifeguard only, could provide a more robust data to calibrate the model. The validation approach proposed here can be applied anywhere pending lifeguard hazard assessment can be performed. If such lifeguard data cannot be collected, a first-pass approach is to base the hazard level scales on the threshold values computed in southwest France (Table 1). Once again, such model application

together with lifeguard-perceived hazard should be tested elsewhere to address the influence of beach state, modal wave climate
270 and lifeguard perception on these threshold values.

Given that shore-break waves cause a large proportion of SZIs in southwest France (Castelle et al., 2018; de Korte et al., 2021; Castelle et al., 2024), we also proposed a shore-break wave hazard forecast model following a similar physics-based approach. Combined, these two surf-zone hazard forecasts can provide detailed insight into surf-zone hazard evolution. This is illustrated in Figure 11 which shows the time series of rip-current velocity V and hazard RHm, and of shore-break wave energy
275 E_{sb} and hazard SHm (Figure 11c,d), for an idealised time series of wave (Figure 11a) and tide (Figure 11b) conditions. For instance, this synthetic test case shows that rip-current flow and shore-break wave energy exhibit an out-of-phase behaviour with, under high-energy conditions (days 3 and 4), high rip-flow velocities sustained throughout the day ($V > 0.7$ m/s). In contrast, even under high-energy waves, shore-break wave energy only peaks during the highest stage of the tide. Therefore, if rip-current hazard gradually increases with increasing wave energy, still with higher hazard for low tide levels, shore-break
280 wave hazard is more modulated by tide, with shore-break wave hazard systematically absent at the lowest stage of the tide, even under high-energy waves (day 3 in Figure 11d).
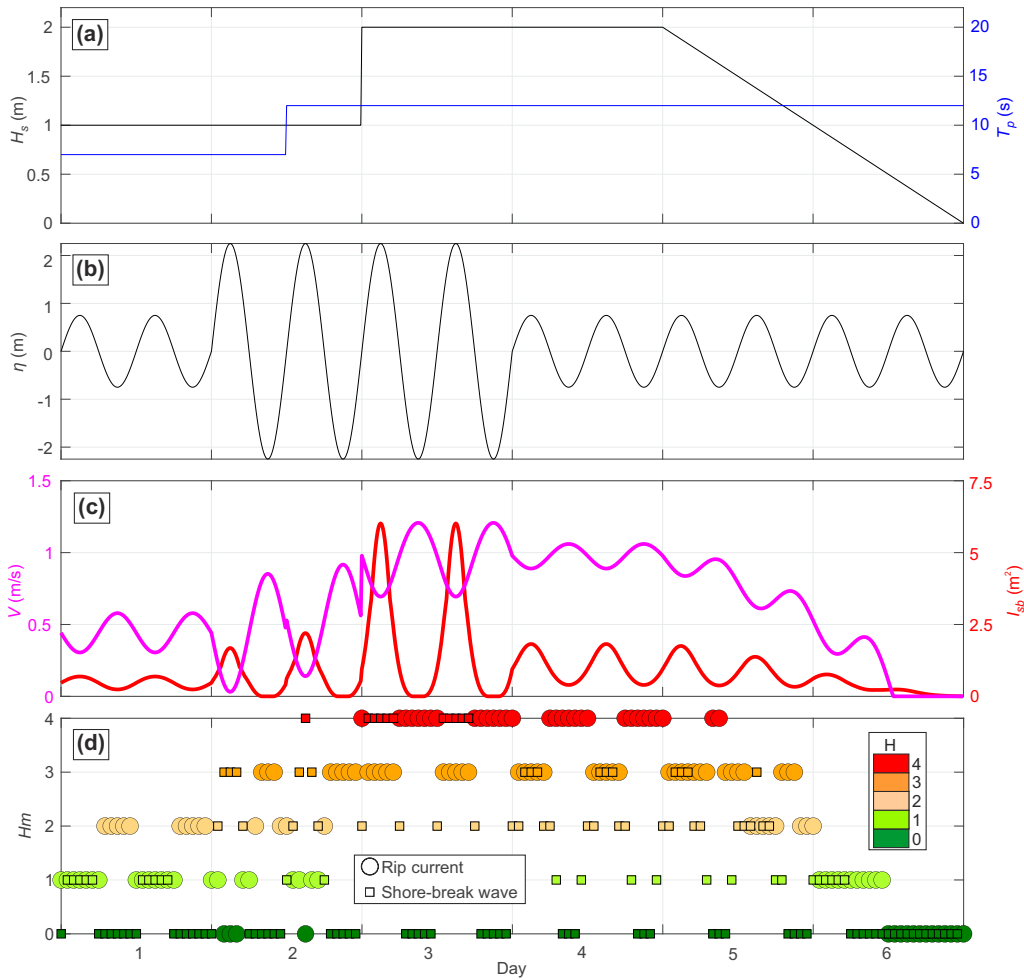
Figure 11. Synthetic time series of (a) offshore significant wave height H_{s0} and peak wave period T_p; (b) astronmical tide level η; (c) modelled rip-flow speed V and shore-break wave intensity I and (d) their hazard level (coloured).

In addition to e.g. the 10-min or hourly rip-current and shore-break wave hazard forecasts, daily-mean hazard levels also showed very good skill, with a pearson correlation with daily-mean lifeguard-perceived hazards of $r = 0.82$ and 0.74 for rip currents and shore-break waves, respectively. However, daily-mean hazard can be predicted with even simpler approach i.e.
285 based on the wave factor defined as $W_f = H_s T_p / |H_s T_p|$ (with the $|.|$ notation the summer mean). By using this number introduced by Scott et al. (2014) to address rip-current rescues in UK, Castelle et al. (2019, 2024) showed that days with large W_f values were associated a disproportionate amount of both rip-current related drowning and shore-break wave related injuries. During the summer 2022, the correlation between daily-mean W_f and daily-mean lifeguard-perceived hazards reaches $R = 0.91$, which outperforms $\overline{RH}m$ ($r = 0.82$). Such improvement is not found with shore-break waves, mostly because
290 daily-mean shore-break wave hazard is much more affected by tidal range than daily-mean rip current hazard (Castelle et al., 2019, 2024). Given that daily-mean rip-current hazard forecast is important in providing a straightforward message to the

general public, the daily-mean wave factor W_f appears as a very simple and powerful way to predict and communicate on high rip-current hazard days. This is complementary to the higher-frequency rip-current hazard prediction during the day with our physics-based model, and to the shore-break hazard model which can be used for both daily-mean and hourly predictions.

295   Instead of using field data, here the models were calibrated based on lifeguard-perceived surf-zone hazard levels. The primary reason was that the bathymetry of La Lette Blanche beach was not surveyed during the summer of 2022, limiting the ability to estimate the bar/rip morphology metrics used in the rip-flow model. Instead, these metrics were found by maximizing the correlation between modelled rip-flow speed V and lifeguard-perceived rip-current hazard RHl. The best model skill was found for bar crest elevation $z_{bar} = -3$ m and channel depth $d = 6.5$ m. These numbers are in line with previous detailed

300   surveys of some bar/rip morphology in southwest France (Sénéchal et al., 2011; Castelle et al., 2018). It must be noted that, while modelled rip-flow velocity is quite sensitive to the choice of the model free parameters, good skill is also found when using values significantly different from the optimal ones. For instance correlation between V and RHl decreased from 0.77 to just 0.75 ($\approx -3\%$) by assuming a higher bar crest ($z_{bar} = -2$ m instead of -3 m) and much shallower channel (d=2 m instead of 6.5 m). Therefore decent model skill can be obtained with a rough estimate of the bar/rip morphology. Similar confusion

305   matrix accuracy were also obtained as the thresholds (Table 1) are modified based a the quantile-quantile approach. For the sake of consistency the free morphological parameters of the shore-break wave model were also found by maximizing the pearson correlation between shore-break wave energy E_{sb} and lifeguard-perceived shore-break wave hazard SHl. When compared to the alongshore-averaged beach topography measured on July 12, 2022 at La Lette Blanche (Figure 12), the Dean profile (solid blued line in Figure 12b) is much steeper than the alongshore-averaged profile. However, by changing a=-2.75 into a=-1.75,

310   which is in much better agreement with the measured profile (dotted blue line in Figure 12b), the correlation between E_{sb} and SHl decreases from R=0.72 to just 0.69 ($\approx -4\%$). This once again shows that beach surveys can be used instead of a Dean profile calibrated with lifeguard-perceived hazards. Overall, both the rip-current and shore-break wave hazard forecast models can be used based on some basic knowledge of the beach morphology.
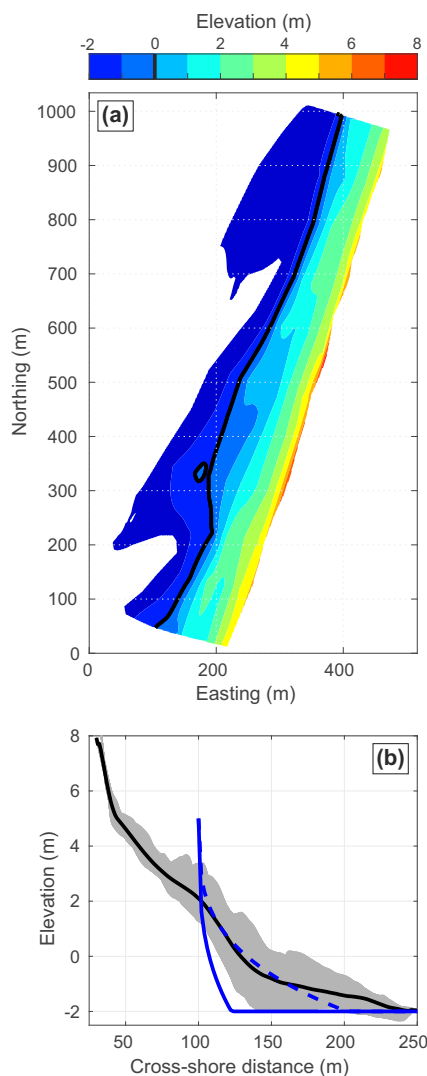
Figure 12. La Lette Blanche beach topographic survey performed at low tide on July 12, 2022 with (a) digital elevation model with elevation with respect to mean sea level coloured and (b) all cross-shore (light grey) and alongshore-averaged (thick black) profiles, with the blue (dotted) blue lines depicting the Dean profile for $a = -2.75$ and $b = 0.3$ ($a = -1.75$ and $b = 0.3$).

In line with (Moulton et al., 2017b), the rip-flow model does not seem to consider the wave period T_p. However, rip-flow
315 speed is known to increase with increasing wave period (Castelle et al., 2020), and we also show that wave period is key to
the wave factor W_f which outperforms daily-mean V in explaining $\overline{RHl}$ variance. Surprisingly enough, including $(T_p/|T_p|)^n$
in Equation (4) did not increase model skill (best correlation was obtained for $n = 0$). However, T_p is indirectly considered
here in our model as the shoaled significant wave height H_s is considered through the formulation of Larson et al. (2010),
resulting in larger breaking wave height for larger period. This is why in Figure 11c the rip flow speed increases by 7% (from
320 0.85 to 0.91 m/s at spring low tide) during day 2 as T_p increases from 7 to 12 s. Replacing the shoaled significant wave height

at breaking H_s by the significant wave height at the Météo-France wave model in nearly 10-m depth H_{s0} slightly decreased the correlation between V and RHl from 0.77 to 0.75, showing the weak but significant and positive influence of wave period T_p on rip flow speed. In addition, under increasingly obliquely-incident waves, rip current tends to progressively change from a symmetric seaward-flowing jet to an undulating longshore current (MacMahan et al., 2010). The influence of the presence

325 of a longshore current component on the decay of rip flow was tested using the same approach as in Moulton et al. (2017a) and Casper et al. (2024). However, inclusion of the longshore current did not improve model skill. This is in agreement with Moulton et al. (2017b) who suggested that for deeper rip channels, like along the southwest France open beaches, rip-flow speed is not suppressed under obliquely incident waves. Including the effect of longshore current on rip flow speed is strongly encouraged if applying the model on beaches with shallow rip channels (MacMahan et al., 2008).

330 The predicted natural hazard level is critical to communicate towards the general public as, by definition, it provides a direct information on the level of threat of a naturally occurring event, here intense rip currents and powerful shore-break waves. However, the number of rescues and SZIs, which is of strong interest for e.g. lifeguard institutions and emergency units as it is the proxy of the volume of activity and thus of man power needs, also depends on the number of people exposing themselves to the physical hazards (the exposure component described in Stokes et al., 2017). An option to predict beach risk is to fit e.g. a

335 logistic regression model with SZIs data based on wave, tide and weather forecasts (Tellier et al., 2022). However, model skill strongly depends on the SZI dataset size and quality, and such model fail to identify the respective contributions of exposure and hazard components to the overall risk. The exposure component can be addressed through beach attendance, which can be computed with different techniques using e.g. video systems (Boominathan et al., 2016; Guillén et al., 2008). Given that beach attendance is largely governed by weather conditions (e.g. Dwight et al., 2007; Moreno et al., 2008; Ibarra, 2011; Coombes

340 et al., 2009), as well as weekday and holiday periods (Kane et al., 2021; Tellier et al., 2022), machine learning techniques (e.g. Mahesh, 2020; Domingo, 2021) can be used to predict beach crowds. In order to robustly link up beach crowds and the number of people entering the water, which is exposure, the bathing rate will need to be addressed. Dwight et al. (2007) have estimated that, on average, only 45% of individuals arriving at the beach have physical contact with water on the southern California beaches. Such a proportion decreases during the colder winter months (26%) and increases in summer during warmer days

345 (54%). Wave conditions can also influence the rate of bathing. For instance, de Korte et al. (2021) found that large shore-break waves ($H_s > 2.5$ m) can deter beachgoers from entering the water. Similarly, Dehez et al. (2024) demonstrated that weather and ocean conditions significantly impact beachgoers' risk perception and, consequently, their likelihood of entering the water. Further research is needed to improve predictions of exposure.

6   Conclusions

350 This paper introduces two new, simple, physics-based rip-current and shore-break wave hazard forecast models. These models, which depend on a limited number of free parameters, allow to compute the time evolution of the rip current flow speed V and shore-break wave energy E_{sb}. Using hourly lifeguard-perceived hazards collected over a two-month period, a quantile-quantile approach was used to transform V and E_{sb} into 5-level scale from 0 (no hazard) to 4 (hazard maximized). The forecast models

accurately predict rip-current and shore-break wave hazard levels, including their modulation by tide elevation and incident
wave conditions, opening new perspectives to forecast multiple surf-zone hazards on sandy beaches. The approach presented
requires only a few basic beach morphology metrics, enabling surf-zone hazard prediction on beaches with wave forecasts.
Combined with global beach safety research, this effort supports the development and communication of surf-zone hazard
forecasts to help reduce drownings and surf-zone injuries.

Data availability. The wave, tide and lifeguard-perceived rip-current and shore-break wave hazard datasets are available at https://osf.io/tzqax/

Author contributions. Conceptualization, data curation, formal analysis, model development, visualization and writing of the original draft
was by BC; JPS collected lifeguard data; SL produced the wave data; Model validation by BC with guidance of DC; All authors reviewed
and edited the draft; Project administration and funding by BC and JD.

Competing interests. The authors declare that they have no conflict of interest

Acknowledgements. This study received financial support from Project SWYM (Surf zone hazards, recreational beach use and Water safetY
Management in a changing climate) funded by Région Nouvelle-Aquitaine and the French government in the framework of the University
of Bordeaux's IdEx "Investments for the Future" program/RRI Tackling Global Change. We warmly thank the SMGBL (Syndicat Mixte
de Gestion des Baignades Landaise), and particularly Stéphanie Barneix and the La Lette Blanche lifeguards who were on duty during the
summer of 2022. We are also thankful to the Vielle Saint-Girons council for providing technical support and access to the lifeguard facilities.

References

370 Aagaard, T., Greenwood, B., and Nielsen, J.: Mean currents and sediment transport in a rip channel, Marine Geology, 140, 25–45, https://doi.org/10.1016/S0025-3227(97)00025-X, 1997.

Arozarena, I., Houser, C., Echeverria, A., and Brannstrom, C.: The rip current hazard in Costa Rica, Natural Hazards, 77, 753–768, https://doi.org/10.1007/s11069-015-1626-9, 2015.

Atkinson, A. L., Power, H. E., Moura, T., Hammond, T., Callaghan, D. P., and Baldock, T. E.: Assessment of runup pre-
375 dictions by empirical models on non-truncated beaches on the south-east Australian coast, Coastal Engineering, 119, 15–31, https://doi.org/https://doi.org/10.1016/j.coastaleng.2016.10.001, 2017.

Austin, M., Scott, T. M., Brown, J. W., Brown, J. A., MacMahan, J. H., Masselink, G., and Russell, P.: Temporal observations of rip current circulation on a macro-tidal beach, Cont. Shelf. Res., 30, 1149–1165, https://doi.org/10.1016/j.csr.2010.03.005, 2010.

Austin, M., Scott, T. M., Russell, P. E., and Masselink, G.: Rip Current Prediction: Development, Validation and Evaluation of an Operational
380 Tool, J. Coast. Res., 29, 283–300, https://doi.org/10.2112/JCOASTRES-D-12-00093.1, 2013.

Barlas, B. and Beji, S.: Rip current fatalities on the Black Sea beaches of Istanbul and effects of cultural aspects in shaping the incidents, Natural Hazards, 80, 811–821, https://doi.org/10.1007/s11069-015-1998-x, 2016.

Bates, P. D., Quinn, N., Sampson, C., Smith, A., Wing, O., Sosa, J., Savage, J., Olcese, G., Neal, J., Schumann, G., Giustarini, L., Coxon, G., Porter, J. R., Amodeo, M. F., Chu, Z., Lewis-Gruss, S., Freeman, N. B., Houser, T., Delgado, M., Hamidi, A., Bolliger, I., E. McCusker, K.,
385 Emanuel, K., Ferreira, C. M., Khalid, A., Haigh, I. D., Couasnon, A., E. Kopp, R., Hsiang, S., and Krajewski, W. F.: Combined Modeling of US Fluvial, Pluvial, and Coastal Flood Hazard Under Current and Future Climates, Water Resources Research, 57, e2020WR028 673, https://doi.org/https://doi.org/10.1029/2020WR028673, 2021.

Battjes, J. A.: Surf similarity, in: 14th Int. Conf. on Coastal Eng., pp. 466–480, ASCE, 1974.

Boominathan, L., Kruthiventi, S., and Venkatesh Babu, R.: CrowdNet: A deep convolutional network for dense crowd counting, pp. 640–644,
390 https://doi.org/10.1145/2964284.2967300, 2016.

Bowen, A. J.: Rip currents: 1. Theoretical investigations, Journal of Geophysical Research (1896-1977), 74, 5467–5478, https://doi.org/https://doi.org/10.1029/JC074i023p05467, 1969.

Brander, R. W. and Short, A. D.: Flow kinematics of low-energy rip current systems, J. Coast. Res., 17, 468–481, 2001.

Brewster, B. C., Gould, R. E., and Brander, R. W.: Estimations of rip current rescues and drowning in the United States, Natural Hazards and
395 Earth System Sciences, 19, 389–397, https://doi.org/10.5194/nhess-19-389-2019, 2019.

Brighton, B., Sherker, S., Brander, R., Thompson, M., and Bradstreet, A.: Rip current related drowning deaths and rescues in Australia 2004–2011, Nat. Hazards Earth Syst. Sci., 13, 1069–1075, https://doi.org/10.5194/nhess-13-1069-2013, 2013.

Britton, E., Kindermann, G., Domegan, C. T., and Carlin, C. M.: Blue care: a systematic review of blue space interventions for health and wellbeing, Health Promotion International, 35, 50 – 69, 2018.

400 Bruneau, N., Castelle, B., Bonneton, P., Pedreros, R., Almar, R., Bonneton, N., Bretel, P., Parisot, J.-P., and Sénéchal, N.: Field observations of an evolving rip current on a meso-macrotidal well-developed inner bar and rip morphology, Continental Shelf Research, 29, 1650–1662, https://doi.org/10.1016/j.csr.2009.05.005, 2009.

Bruneau, N., Bonneton, P., Castelle, B., and Pedreros, R.: Modeling rip current circulations and vorticity in a high-energy mesotidal-macrotidal environment, J. Geophys. Res. Oceans, 116, https://doi.org/10.1029/2010JC006693, 2011.

405   Brunner, M. I., Slater, L., Tallaksen, L. M., and Clark, M.: Challenges in modeling and predicting floods and droughts: A review, WIREs Water, 8, e1520, https://doi.org/https://doi.org/10.1002/wat2.1520, 2021.

Bujosa, A., Riera, A., and Pons, P. J.: Sun-and-beach tourism and the importance of intra-destination movements in mature destinations, Tourism Geographies, 17, 780–794, https://doi.org/10.1080/14616688.2015.1093538, 2015.

Casper, A., Nuss, E. S., Baker, C. M., Moulton, M., and Dusek, G.: Assessing NOAA Rip-Current Hazard Likelihood Predictions: Com-
410   parison with Lifeguard Observations and Parameterizations of Bathymetric and Transient Rip-Current Types, Weather and Forecasting, 2024.

Castelle, B., Scott, T., Brander, R., and McCarroll, R.: Rip current types, circulation and hazard, Earth Sci. Rev., 163, 1–21, https://doi.org/10.1016/j.earscirev.2016.09.008, 2016.

Castelle, B., Brander, R., Tellier, E., Simonnet, B., Scott, T., McCarroll, J., Campagne, J.-M., Cavailhes, T., and Lechevrel, P.: Surf zone
415   hazards and injuries on beaches in SW France, Nat. Hazards, 93, 1317–1335, https://doi.org/10.1007/s11069-018-3354-4, 2018.

Castelle, B., Scott, T., Brander, R., McCarroll, J., Robinet, A., Tellier, E., de Korte, E., Simonnet, B., and Salmi, L.-R.: Environmental controls on surf zone injuries on high-energy beaches., Nat. Hazards Earth Syst. Sci., 19, https://doi.org/10.5194/nhess-19-2183-2019, 2019.

Castelle, B., Scott, T., Brander, R., McCarroll, R., Tellier, E., De Korte, E., Tackuy, L., Robinet, A., Simonnet, B., and Salmi, L.-R.: Wave
420   and Tide Controls on Rip Current Activity and Drowning Incidents in Southwest France, Journal of Coastal Research, 95, 769–774, https://doi.org/10.2112/SI95-150.1, 2020.

Castelle, B., Dehez, J., Savy, J.-P., Marieu, V., Lyser, S., Bujan, S., Carayon, D., and Brander, R.: Environmental controls on lifeguard-estimated surf-zone hazards, beach crowds, and resulting life risk at a high-energy sandy beach in southwest France, Natural Hazards: Journal of the International Society for the Prevention and Mitigation of Natural Hazards, 120, 1557–1576, https://doi.org/10.1007/s11069-
425   023-06250-, 2024.

Chang, S. K. Y., Tominaga, G. T., Wong, J. H., Weldon, E. J., and Kaan, K. T.: Risk factors for water sports-related cervical spine injuries., The Journal of trauma, 60 5, 1041–1046, 2006.

Coombes, E., Jones, A. P., Bateman, I., Tratalos, J., Gill, J., Showler, D., Watkinson, A., and Sutherland, W.: Spatial and temporal modeling of beach use: A case study of east Anglia, UK, Coastal Management, 37, 94 – 115, https://doi.org/10.1080/08920750802527127, 2009.

430   Corral, C., Berenguer, M., Sempere-Torres, D., Poletti, L., Silvestro, F., and Rebora, N.: Comparison of two early warning systems for regional flash flood hazard forecasting, Journal of Hydrology, 572, 603–619, https://doi.org/https://doi.org/10.1016/j.jhydrol.2019.03.026, 2019.

Dalrymple, R. A., MacMahan, J. H., Reniers, A. J., and Nelko, V.: Rip Currents, Annu. Rev. Fluid Mech., 43, 551–581, https://doi.org/10.1146/annurev-fluid-122109-160733, 2011.

435   de Korte, E., Castelle, B., and Tellier, E.: A Bayesian network approach to modelling rip-current drownings and shore-break wave injuries, Natural Hazards and Earth System Sciences, 21, 2075–2091, https://doi.org/10.5194/nhess-21-2075-2021, 2021.

Dehez, J. and Lyser, S.: How ocean beach recreational quality fits with safety issues? An analysis of risky behaviours in France, Journal of Outdoor Recreation and Tourism, 45, 100 711, https://doi.org/https://doi.org/10.1016/j.jort.2023.100711, 2024.

Dehez, J., Lyser, S., Castelle, B., Brander, R. W., Peden, A. E., and Savy, J. P.: Investigating beachgoer's perception of coastal bathing risks
440   in southwest France, Natural Hazards, https://doi.org/10.1007/s11069-024-06715-w, 2024.

Domingo, M. C.: Deep Learning and Internet of Things for Beach Monitoring: An Experimental Study of Beach Attendance Prediction at Castelldefels Beach, Applied Sciences, 2021.

Drozdzewski, D., Shaw, W., Dominey-Howes, D., Brander, R., Walton, T., Gero, A., Sherker, S., Goff, J., and Edwick, B.: Surveying rip current survivors: preliminary insights into the experiences of being caught in rip currents, Nat. Hazards Earth Syst. Sci., 12, 1201–1211, https://doi.org/10.5194/nhess-12-1201-2012, 2012.

445 Drønen, N., Karunarathna, H., Fredsøe, J., Mutlu Sumer, B., and Deigaard, R.: An experimental study of rip channel flow, Coastal Engineering, 45, 223–238, https://doi.org/https://doi.org/10.1016/S0378-3839(02)00035-2, 2002.

Dusek, G. and Seim, H.: Rip Current Intensity Estimates from Lifeguard Observations, Journal of Coastal Research, 29, 505–518, https://doi.org/10.2112/JCOASTRES-D-12-00117.1, 2012.

450 Dusek, G. and Seim, H.: A probabilistic rip current forecast model, J. Coast. Res., 29, 909–925, https://doi.org/10.2112/JCOASTRES-D-12-00118.1, 2013.

Dwight, R. H., Brinks, M. V., SharavanaKumar, G., and Semenza, J. C.: Beach attendance and bathing rates for Southern California beaches, Ocean Coast. Manage., 50, 847 – 858, https://doi.org/10.1016/j.ocecoaman.2007.04.002, 2007.

Egbert, G. D. and Erofeeva, S. Y.: Efficient Inverse Modeling of Barotropic Ocean Tides, Journal of Atmospheric and Oceanic Technology,
455 19, 183 – 204, https://doi.org/10.1175/1520-0426(2002)019<0183:EIMOBO>2.0.CO;2, 2002.

Gall, R. L., Franklin, J. L., Marks, F., Rappaport, E. N., and Toepfer, F.: The Hurricane Forecast Improvement Project, Bulletin of the American Meteorological Society, 94, 329–343, 2013.

Ghermandi, A. and Nunes, P. A.: A global map of coastal recreation values: Results from a spatially explicit meta-analysis, Ecological Economics, 86, 1 – 15, https://doi.org/10.1016/j.ecolecon.2012.11.006, 2013.

460 Gomes da Silva, P., Coco, G., Garnier, R., and Klein, A. H.: On the prediction of runup, setup and swash on beaches, Earth-Science Reviews, 204, 103 148, https://doi.org/https://doi.org/10.1016/j.earscirev.2020.103148, 2020.

Griepp, D. W., de la Garza Ramos, R., Lee, J., Miller, A., Prasad, M., Gelfand, Y., Cardozo-Stolberg, S., and Murthy, S.: Beach Breaking Waves and Related Cervical Spine Injuries: A Level One Trauma Center Experience and Systematic Review, World Neurosurgery, 160, e471–e480, https://doi.org/https://doi.org/10.1016/j.wneu.2022.01.055, 2022.

465 Guillén, J., García-Olivares, A., Ojeda, E., Osorio, A., Chic, O., and González, R.: Long-term quantification of beach users using video monitoring, Journal of Coastal Research, 24, 1612–1619, https://doi.org/10.2112/07-0886.1, 2008.

Guza, R. T. and Thornton, E. B.: Wave set-up on a natural beach, Journal of Geophysical Research: Oceans, 86, 4133–4137, https://doi.org/https://doi.org/10.1029/JC086iC05p04133, 1981.

Hall, C. M. and Page, S. J.: The Geography of Tourism and Recreation: Environment, Place and Space,
470 https://doi.org/10.4324/9780203796092, 2014.

Haller, M. C., Dalrymple, R. A., and Svendsen, I. A.: Experimental study of nearshore dynamics on a barred beach with rip channels, Journal of Geophysical Research: Oceans, 107, 14–1–14–21, https://doi.org/https://doi.org/10.1029/2001JC000955, 2002.

Houser, C., Arnott, R., Ulzhofer, S., and Barrett, G.: Nearshore circulation over transverse bar and rip morphology with oblique wave forcing, Earth Surf. Process. Landf., 38, 1269–1279, https://doi.org/10.1002/esp.3413, 2013.

475 Houser, C., Wernette, P., Trimble, S., and Locknick, S.: 11 - Rip currents, in: Sandy Beach Morphodynamics, edited by Jackson, D. W. and Short, A. D., pp. 255–276, Elsevier, https://doi.org/https://doi.org/10.1016/B978-0-08-102927-5.00011-4, 2020.

Ibarra, E.: The use of webcam images to determine tourist-climate aptitude: Favourable weather types for sun and beach tourism on the Alicante coast (Spain), Int. J. Biometeorol., 55, 373–385, https://doi.org/10.1007/s00484-010-0347-8, 2011.

Kane, B., Zajchowski, C. A., Allen, T. R., McLeod, G., and Allen, N. H.: Is it safer at the beach? Spatial and temporal analyses of beachgoer behaviors during the COVID-19 pandemic, Ocean & Coastal Management, 205, 105 533, https://doi.org/https://doi.org/10.1016/j.ocecoaman.2021.105533, 2021.

Larson, M., Hoan, L. X., and Hanson, H.: Direct Formula to Compute Wave Height and Angle at Incipient Breaking, Journal of Waterway Port Coastal and Ocean Engineering-asce, 136, 119–122, 2010.

Li, Z.: Rip current hazards in South China headland beaches, Ocean & Coastal Management, 121, 23–32, https://doi.org/https://doi.org/10.1016/j.ocecoaman.2015.12.005, 2016.

MacMahan, J., Brown, J., Brown, J., Thornton, E., Reniers, A., Stanton, T., Henriquez, M., Gallagher, E., Morrison, J., Austin, M. J., Scott, T. M., and Senechal, N.: Mean Lagrangian flow behavior on an open coast rip-channeled beach: A new perspective, Marine Geology, 268, 1–15, https://doi.org/https://doi.org/10.1016/j.margeo.2009.09.011, 2010.

MacMahan, J. H., Thornton, E. B., Stanton, T. P., and Reniers, A. J. H. M.: RIPEX-observations of a rip current system, Mar. Geol., 218, 113–134, https://doi.org/10.1016/j.margeo.2005.03.019, 2005.

MacMahan, J. H., Thornton, E. B., and Reniers, A. J. H. M.: Rip current review, Coast. Eng., 53, 191–208, https://doi.org/10.1016/j.coastaleng.2005.10.009, 2006.

MacMahan, J. H., Thornton, E. B., Reniers, A. J., Stanton, T. P., and Symonds, G.: Low-Energy Rip Currents Associated With Small Bathymetric Variations, Mar. Geol., 255, 156 – 164, https://doi.org/10.1016/j.margeo.2008.08.006, 2008.

Mahesh, B.: Machine learning algorithms-a review, International Journal of Science and Research, 9, 381–386, 2020.

Merz, B., Kuhlicke, C., Kunz, M., Pittore, M., Babeyko, A., Bresch, D. N., Domeisen, D. I. V., Feser, F., Koszalka, I., Kreibich, H., Pantillon, F., Parolai, S., Pinto, J. G., Punge, H. J., Rivalta, E., Schröter, K., Strehlow, K., Weisse, R., and Wurpts, A.: Impact Forecasting to Support Emergency Management of Natural Hazards, Reviews of Geophysics, 58, e2020RG000 704, https://doi.org/https://doi.org/10.1029/2020RG000704, 2020.

Moreno, Á., Amelung, B., and Santamarta, L.: Linking beach recreation to weather conditions: a case study in Zandvoort, Netherlands., Tourism in Marine Environments, 5, 111–119, 2008.

Moulton, M., Dusek, G., Elgar, S., and Raubenheimer, B.: Comparison of Rip Current Hazard Likelihood Forecasts with Observed Rip Current Speeds, Weather and Forecasting, 32, 1659–1666, 2017a.

Moulton, M., Elgar, S., Raubenheimer, B., Warner, J. C., and Kumar, N.: Rip currents and alongshore flows in single channels dredged in the surf zone, Journal of Geophysical Research: Oceans, 122, 3799–3816, https://doi.org/https://doi.org/10.1002/2016JC012222, 2017b.

National Research Council: A Safer Future: Reducing the Impacts of Natural Disasters, The National Academies Press, Washington, DC, https://doi.org/10.17226/1840, 1991.

Puleo, J., Hutschenreuter, K., Cowan, P., Carey, W., Arford-Granholm, M., and McKenna, K.: Delaware surf zone injuries and associated environmental conditions, Nat. Hazards, 81, 845–867, https://doi.org/10.1007/s11069-015-2108-9, 2016.

Raubenheimer, B., Guza, R. T., and Elgar, S.: Field observations of wave-driven setdown and setup, Journal of Geophysical Research: Oceans, 106, 4629–4638, https://doi.org/https://doi.org/10.1029/2000JC000572, 2001.

Robbles, L.: Cervical spine injuries in ocean bathers: wave-related accidents, Neurosurgery, 58, 920–923, https://doi.org/10.1227/01.NEU.0000209941.18102.35, 2006.

Roland, A. and Ardhuin, F.: On the developments of spectral wave models: numerics and parameterizations for the coastal ocean, Ocean Dynamics, 64, 833–846, 2014.

Rowe, G. and Wright, G.: Differences in Expert and Lay Judgments of Risk: Myth or Reality?, Risk Analysis, 21, 341–356, https://doi.org/https://doi.org/10.1111/0272-4332.212116, 2001.

Sandman, P. M., Weinstein, N. D., and Klotz, M. L.: Public Response to the Risk from Geological Radon, Journal of Communication, 37, 93–108, https://doi.org/https://doi.org/10.1111/j.1460-2466.1987.tb00997.x, 1987.

520 Scott, T., Masselink, G., Austin, M. J., and Russell, P.: Controls on macrotidal rip current circulation and hazard, Geomorphology, 214, 198–215, https://doi.org/10.1016/j.geomorph.2014.02.005, 2014.

Scott, T., Masselink, G., Stokes, C., Poate, T., Wooler, A., and Instance, S.: A 15-year partnership between UK coastal scientists and the international beach lifeguard community, Continental Shelf Research, 241, 104 732, https://doi.org/https://doi.org/10.1016/j.csr.2022.104732, 2022.

525 Sénéchal, N., Abadie, S., Gallagher, E., MacMahan, J. H., Masselink, G., Michallet, H., Reniers, A. J., Ruessink, G., Russell, P. E., Sous, D., Turner, I. M., Ardhuin, F., Bonneton, P., Bujan, S., Capo, S., Certain, R., Pedreros, R., and Garlan, T.: The ECORS-Truc Vert'08 nearshore field experiment: presentation of a three-dimensional morphologic system in a macro-tidal environment during consecutive extreme storm conditions, Ocean Dynamics, 61, 2073–2098, 2011.

Slovic, P.: Trust, Emotion, Sex, Politics, and Science: Surveying the Risk-Assessment Battlefield, Risk Analysis, 19, 689–701,
530 https://doi.org/https://doi.org/10.1111/j.1539-6924.1999.tb00439.x, 1999.

Stockdon, H. F., Long, J. W., Palmsten, M. L., van der Westhuysen, A. J., Doran, K. S., and Snell, R. J.: Operational forecasts of wave-driven water levels and coastal hazards for US Gulf and Atlantic coasts, Communications Earth & Environment, 2023.

Stokes, C., Masselink, G., Revie, M., Scott, T., Purves, D., and Walters, T.: Application of multiple linear regression and Bayesian belief network approaches to model life risk to beach users in the UK, Ocean & Coast. Manage., 139, 12 – 23,
535 https://doi.org/10.1016/j.ocecoaman.2017.01.025, 2017.

Tellier, E., Simonnet, B., Gil-Jardiné, C., Lerouge-Bailhache, M., Castelle, B., and Salmi, R.: Predicting drowning from sea and weather forecasts: Development and validation of a model on surf beaches of southwestern France, Injury Prevention, 28, 16–22, https://doi.org/10.1136/injuryprev-2020-044092, 2022.

Thom, O., Roberts, K., Leggat, P. A., Devine, S., Peden, A. E., and Franklin, R. C.: Cervical spine injuries occurring at the beach: epidemi-
540 ology, mechanism of injury and risk factors, BMC Public Health, 22, 2022.

Tolman, H. L., Balasubramaniyan, B., Burroughs, L. D., Chalikov, D., Chao, Y. Y., Chen, H. S., and Gerald, V. M.: Development and Implementation of Wind-Generated Ocean Surface Wave Modelsat NCEP, Weather and Forecasting, 17, 311–333, 2002.

US Department of Commerce, N.: Weather related fatality and injury statistics, https://www.weather.gov/hazstat/.

West, N.: Beach Use and Behaviors, pp. 307–311, Springer International Publishing, https://doi.org/10.1007/978-3-319-93806-6_43, 2019.

545 Winter, G., van Dongeren, A., de Schipper, M., and van Thiel de Vries, J.: Rip currents under obliquely incident wind waves and tidal longshore currents, Coastal Engineering, 89, 106–119, https://doi.org/https://doi.org/10.1016/j.coastaleng.2014.04.001, 2014.

Wood, L. E., Vimercati, G., Ferrini, S., and Shackleton, R. T.: Perceptions of ecosystem services and disservices associated with open water swimming, Journal of Outdoor Recreation and Tourism, https://api.semanticscholar.org/CorpusID:247344535, 2022.

Wright, L. D. and Short, A. D.: Morphodynamic variability of surf zones and beaches: A synthesis, Marine Geology, 56, 93–118, 1984.

550 Zscheischler, J., Martius, O., Westra, S., Bevacqua, E., Raymond, C., Horton, R. M., van den Hurk, B., Aghakouchak, A., Jézéquel, A., Mahecha, M. D., Maraun, D., Ramos, A. M., Ridder, N. N., Thiery, W., and Vignotto, E.: A typology of compound weather and climate events, Nature Reviews Earth & Environment, 1, 333 – 347, 2020.